Inorganic Chemistry

Article

pubs.acs.org/IC

Structure and Magnetic Properties of $BiFe_{1-x}Co_xO_3$ and $Bi_{0.9}Sm_{0.1}Fe_{1-x}Co_xO_3$

Makoto Kubota,*[†,‡] Kengo Oka,[‡] Hisato Yabuta,[†] Kaoru Miura,[†] and Masaki Azuma[‡]

[†]Corporate R&D Headquarters, Canon Inc., 3-30-2 Shimomaruko, Ota-ku, Tokyo 146-8501, Japan

[‡]Materials and Structures Laboratory, Tokyo Institute of Technology, 4259 Nagatsuta, Midori-ku, Yokohama 226-8503, Japan

Supporting Information

ABSTRACT: $BiFe_{1-x}Co_xO_3$ and $Bi_{0.9}Sm_{0.1}Fe_{1-x}Co_xO_3$ were synthesized under a high pressure of 4 GPa; 10% Sm substitution for Bi in $BiFe_{1-x}Co_xO_3$ ($x \leq 0.20$) drastically destabilized the ferroelectric $BiFeO_3$-type structure and changed it to an antiferroelectric $PbZrO_3$-type superstructure. In comparison, a ferroelectric $BiCoO_3$-type tetragonal structure ($x \geq 0.40$) was insensitive to the Sm substitution. No decrease in the ferroelectric Curie temperature (T_C) was observed. Weak ferromagnetism with a spontaneous moment of 0.025 μ_B/formula unit (f.u.) was observed for $BiFe_{1-x}Co_xO_3$ (x = 0.10 and 0.20) samples, suggesting the change in the spin structure from a cycloidal one. Because of the coexistence of ferroelectricity and ferromagnetism at room temperature, this compound is a promising multiferroic material.

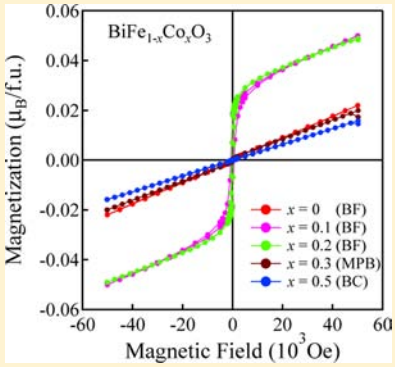

INTRODUCTION

$BiFeO_3$ (BFO) has recently been actively studied as a promising candidate for the constitution of a Pb-free ferroelectric/piezoelectric material.[1] BFO is a perovskite-type oxide with a polar distortion along the [111] direction of the cubic unit cell below a T_C of 850 °C,[2] so the crystal symmetry is rhombohedral with space group $R3c$ and the following lattice parameters: a = 5.579 Å and c = 13.869 Å (hexagonal setting).[3] Although BFO shows a large spontaneous polarization of ∼100 $\mu C/cm^2$,[4] its piezoelectric constant (d_{33} ∼ 60 pm/V)[5] is far smaller than that of Pb-containing piezoelectric materials like $PbZr_{1-x}Ti_xO_3$ (PZT). The largest piezoelectric response of PZT is achieved at the morphotropic phase boundary (MPB) between the rhombohedral and tetragonal phases at around x = 0.5.[6]

Some investigations have followed the PZT system, the solid solutions between rhombohedral BFO and tetragonal Bi based perovskite with a large c/a ratio, e.g., $BiCoO_3$ (c/a = 1.267)[7−15] and $BiZn_{0.5}Ti_{0.5}O_3$ (c/a = 1.211).[16,17] These studies are classified as B-site substitution of the perovskite oxide. Among them, a MPB with a $\sqrt{2}a \times \sqrt{2}a \times a$ monoclinic Cm structure, where a was a lattice constant of a cubic perovskite that was essentially the same as that of PZT, was found in $BiFe_{1-x}Co_xO_3$ with x ∼ 0.3 synthesized under high pressure.[7,8] In the vicinity of the MPB composition, the polarization vector of $BiFe_{1-x}Co_xO_3$ rotates as a function of composition and temperature.[8] In comparison, the large c/a ratio of the tetragonal and monoclinic phases hindered the observation of polarization switching. Another problem is a high T_C of ∼700 °C. It was reported for several systems that a decrease in T_C resulted in an increase in the piezoelectric coefficient.[18−20] Also, the decrease in the c/a ratio is expected to reduce the potential barrier and may allow the observation of polarization switching.[21]

There are several reports on rare earth substitution for Bi^{3+} in the A-site of $BiFeO_3$, as well. Thin films of $Bi_{1-x}Sm_xFeO_3$ fabricated by pulsed laser deposition have maxima in the dielectric and piezoelectric constants at approximately x = 0.14.[22] These enhancements are attributed to a phase transition from the $R3c$ $BiFeO_3$-type structure to another structure.[23−27] We investigated the structural change in Sm-substituted BFO on phase pure bulk samples prepared by high-pressure synthesis. Precise structural analysis based on synchrotron X-ray powder diffraction showed that $Bi_{1-x}Sm_xFeO_3$ ($0.10 \leq x \leq 0.20$) had a $PbZrO_3$-type structure with $\sqrt{2}a \times 2\sqrt{2}a \times 4a$ unit cells.[28] The antipolar $PbZrO_3$-type structure of $Bi_{1-x}Sm_xFeO_3$ changed to a polar $BiFeO_3$-type structure above 160 °C for x = 0.10 and 230 °C for x = 0.12, and the polar structure further changed to a nonpolar $GdFeO_3$-type structure above 506 °C for x = 0.10 and 349 °C for x = 0.12 upon heating, meaning that the Sm substitution markedly lowered the T_C of BFO.[29] Motivated by this finding, we studied the effect of Sm substitution on the structural evolution of $BiFe_{1-x}Co_xO_3$.

Another interesting facet of BFO is its magnetism. It is an antiferromagnet with a T_N of 370 °C, well above room temperature.[30] A cycloidal space-modulated spin structure with a periodicity of 62 nm is superimposed on the G-type antiferromagnetic structure. This spin structure is the same as that of $TbMnO_3$, where electric polarization induced by magnetic ordering was first found.[31,32] Indeed, a sharp change

Received: August 7, 2013
Published: September 4, 2013

in electric polarization is observed in a magnetic field of 18 T for a single-domain crystal of $BiFeO_3$[33] because of the change in the spin structure to a collinear one.[34] A recent polarized small-angle neutron scattering study revealed the presence of local magnetization of 0.06 μ_B/Fe due to spin canting.[35] However, the presence of a spin density wave resulting from cycloidal ordering prohibits the appearance of net ferromagnetic magnetization and a linear magnetoelectric effect. Modifying the spin structure is therefore the key goal for realizing $BiFeO_3$-based ferromagnetic ferroelectrics. For $BiFe_{1-x}Mn_xO_3$ synthesized under high pressure, a structural change from a $BiFeO_3$-type to an antiferroelectric $PbZrO_3$-type structure with $\sqrt{2}a \times 2\sqrt{2}a \times 4a$ unit cells and the appearance of a net ferromagnetic moment due to spin canting were reported.[36−38]

In this paper, we report the structural and magnetic evolutions of Sm- and Co-cosubstituted BFO bulk ceramics. Although it was reported that Sm- and Co-substituted BFO prepared at ambient pressure had a considerable amount of impurity phases over a wide range of calcination temperatures,[39] a series of high-pressure syntheses at 4 GPa allowed us to obtain phase pure samples with various Co compositions. For the purpose of discussion, the Sm ratio was fixed at 0 and 10%, and their structural phase transitions as a function of composition and temperature and their magnetic property at room temperature (RT) were investigated.

EXPERIMENTAL SECTION

$BiFe_{1-x}Co_xO_3$ (x = 0, 0.10, 0.20, 0.30, 0.50, and 0.60) and $Bi_{0.9}Sm_{0.1}Fe_{1-x}Co_xO_3$ (x = 0, 0.05, 0.10, 0.20, 0.30, 0.35, 0.40, 0.45, 0.50, and 0.60) samples were prepared from Bi_2O_3, Sm_2O_3, Fe_2O_3, and Co_3O_4. The bismuth oxide reagent was prebaked overnight at 300 °C. The stoichiometric mixtures were charged in gold capsules 3.6 mm in diameter and 5 mm in height and were compressed to 3 GPa (BFO) or 4 GPa followed by heat treatment at 1000 °C for $BiFe_{1-x}Co_xO_3$ and 850 °C for Sm-substituted samples for 30 min in a cubic anvil-type high-pressure apparatus. Ten milligrams of oxidizing agent $KClO_4$ was added to the top and bottom of the capsule in a separate manner. XRD data were collected at RT on a Bruker D8 Advance diffractometer by using Cu Kα radiation (2θ range of 5−80°, step width of 0.02°, counting time of 0.5 s/step). Synchrotron X-ray powder diffraction (SXRD) data were recorded on a large Debye−Scherrer camera installed at the BL02B2 beamline of SPring-8 in a temperature range of 25−650 °C for precise phase identification and for structural analysis. The incident beam from a bending magnet was monochromatized to a λ of 0.41918 Å. The SXRD data were recorded on an imaging plate with a step interval of 0.01°. The software Rietan-FP was used in the structure refinement.[40] Isothermal magnetization measurements were performed from 50 to −50 kOe and from −50 to 50 kOe at RT with a Quantum Design MPMS XL SQUID magnetometer.

RESULTS AND DISCUSSION

The composition dependencies of the XRD patterns of $BiFe_{1-x}Co_xO_3$ (x = 0, 0.10, 0.20, 0.30, 0.50, and 0.60) and $Bi_{0.9}Sm_{0.1}Fe_{1-x}Co_xO_3$ (x = 0, 0.05, 0.10, 0.20, 0.30, 0.35, 0.40, 0.45, 0.50, and 0.60) at RT are shown in panels a and b of Figure 1, respectively. The compositional phase transition of $BiFe_{1-x}Co_xO_3$ from a rhombohedral $BiFeO_3$-type structure ($0 \le x \le 0.20$) to a monoclinic one (x = 0.30) and eventually to a tetragonal $BiCoO_3$-type structure ($0.50 \le x \le 0.60$) was observed as the Co content increased in agreement with the previous studies.[7,8] $Bi_{0.9}Sm_{0.1}FeO_3$ (x = 0) had a $PbZrO_3$-type *Pnam* $\sqrt{2}a \times 2\sqrt{2}a \times 4a$ structure.[28,29,41] Co-containing samples ($Bi_{0.9}Sm_{0.1}Fe_{1-x}Co_xO_3$ for which $0.05 \le x \le 0.35$) had a $BiFeO_3$-type phase as a minor phase identified by the Rietveld refinement as described below, although their main phase

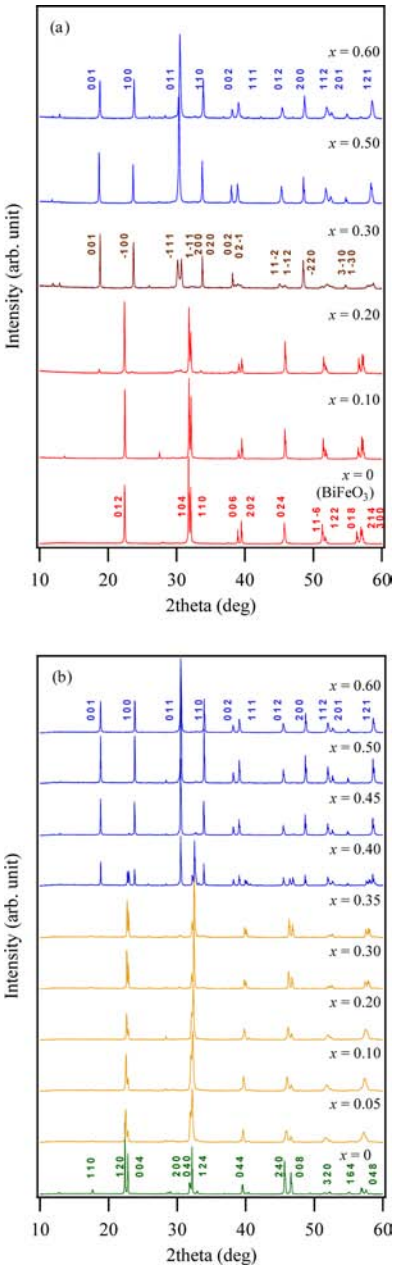

Figure 1. Powder X-ray diffraction patterns of (a) $BiFe_{1-x}Co_xO_3$ (x = 0, 0.10, 0.20, 0.30, 0.50, and 0.60) and (b) $Bi_{0.9}Sm_{0.1}Fe_{1-x}Co_xO_3$ (x = 0, 0.05, 0.10, 0.20, 0.30, 0.35, 0.40, 0.45, 0.50, and 0.60) at room temperature. For the $BiFeO_3$-type phase, the Miller index of the hexagonal system is noted.

remained the $PbZrO_3$-type structure. In comparison, the samples for which $0.45 \le x \le 0.60$ had a $BiCoO_3$-type tetragonal structure like that of Co-rich $BiFe_{1-x}Co_xO_3$. Both the $PbZrO_3$- and $BiCoO_3$-type phases coexisted at the phase boundary (x = 0.40). No monoclinic *Cm* phase was found for the Sm-substituted samples.

To further clarify the phases contained in the mixed phase sample, Rietveld analysis was performed on the SXRD pattern of $Bi_{0.9}Sm_{0.1}Fe_{0.8}Co_{0.2}O_3$ at RT. As shown in Figure 2, the SXRD pattern was successfully fitted by assuming a mixture of the *Pnam* $PbZrO_3$-type phase (67%) and the *R*3*c* phase (33%), just like Mn-substituted BFO.[38] The refined *Pnam* structure is shown in Figure 3 with the structural parameters summarized

dx.doi.org/10.1021/ic402041p | *Inorg. Chem.* 2013, 52, 10698−10704

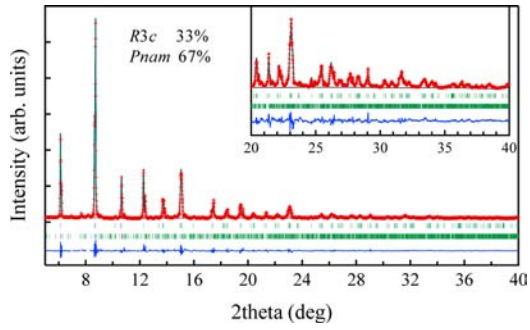

Figure 2. Observed, calculated, and difference synchrotron X-ray powder diffraction (SXRD) patterns of $Bi_{0.9}Sm_{0.1}Fe_{0.8}Co_{0.2}O_3$ at room temperature. The wavelength (λ) was 0.41918 Å. Bars mark reflection positions (from top to bottom) for *R*3*c* and *Pnam* phases.

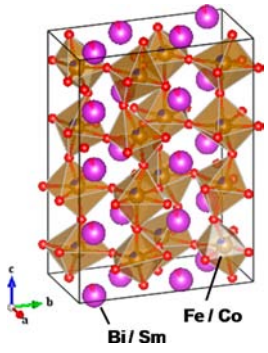

Figure 3. Refined crystal structure of the *Pnam* phase of $Bi_{0.9}Sm_{0.1}Fe_{0.8}Co_{0.2}O_3$.

in Table 1. The isotropic atomic displacement parameters for oxygen sites were fixed at $B = 1$ during the refinement. $PbZrO_3$ has a *Pbam* $\sqrt{2}a \times 2\sqrt{2}a \times 2a$ structure where Pb and Zr ions shift in the *a*-direction in an antiferroelectric manner, leading to the doubling of the *b*-axis. The present $\sqrt{2}a \times 2\sqrt{2}a \times 4a$ structure had further doubling of the unit cells along the *c*-direction. The lattice parameters of the *Pnam* phase were as follows: $a = 5.5280(4)$ Å, $b = 11.1335(6)$ Å, and $c = 15.5243(6)$ Å (all smaller than those of $Bi_{0.9}Sm_{0.1}FeO_3$,[28,29] attributed to B-site substitution). The lattice parameters of the *R*3*c* phase were as follows: $a = 5.5354(1)$ Å and $c = 13.6585(3)$ Å (also smaller than those of BFO).[3]

The lattice parameters of $Bi_{0.9}Sm_{0.1}Fe_{1-x}Co_xO_3$ refined by Rietveld analysis of the SXRD data ($x = 0$, 0.20, and 0.30) and the laboratory XRD data ($x = 0.45$, 0.50, and 0.60) are summarized in Figure 4 with the c/a ratio (only for the tetragonal phase) and unit cell volume. All error bars are hidden behind the corresponding symbols. For comparison, the lattice parameters of the $PbZrO_3$- and $BiFeO_3$-type unit cells were reduced to those of perovskite unit cells. Two sets of data are plotted for $x = 0.20$ and 0.30 because of the coexistence of $PbZrO_3$- and $BiFeO_3$-type phases. It is shown that the lattice parameters of the $PbZrO_3$- and $BiFeO_3$-type phase decreased as

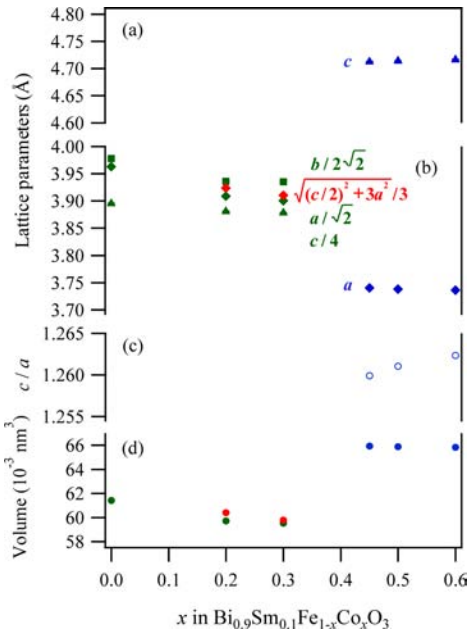

Figure 4. Composition dependence of the lattice parameters, c/a ratio, and unit cell volume of $Bi_{0.9}Sm_{0.1}Fe_{1-x}Co_xO_3$ at room temperature. Green, red, and blue symbols represent data for $PbZrO_3$-, $BiFeO_3$-, and $BiCoO_3$-type structures, respectively. Lattice parameters of $PbZrO_3$- and $BiFeO_3$-type phases are reduced to those of cubic perovskite unit cells.

Table 1. Structural Parameters for $Bi_{0.9}Sm_{0.1}Fe_{0.8}Co_{0.2}O_3$ Refined by Rietveld Analysis of SXRD Patterns Collected at Room Temperature

phase	model	cell (Å)	atom	Wyck	*x*	*y*	*z*	*B*	*R* factor (%)
67%	*Pnam*	$a = 5.5280(4)$	Bi/Sm1	8d	0.2437(11)	0.8704(9)	0.0091(2)	1.22(2)	$R_{wp} = 6.370$
		$b = 11.1335(6)$	Bi/Sm2	4c	0.2699(28)	0.3766(11)	0.25	1.22(2)	$R_B = 2.249$
		$c = 15.5243(6)$	Bi/Sm3	4c	0.2127(24)	0.8791(11)	0.25	1.22(2)	
			Fe1/Co1	8d	0.2197(42)	0.6147(26)	0.1272(13)	0.49(7)	
			Fe2/Co2	8d	0.2486(64)	0.6263(33)	0.6190(13)	0.49(7)	
			O1	8d	0.2772(146)	0.5811(54)	0.9959(11)	1	
			O2	4c	0.8118(257)	0.3642(123)	0.25	1	
			O3	8d	0.4455(155)	0.9854(91)	0.1439(63)	1	
			O4	8d	0.5421(130)	0.5357(41)	0.1299(73)	1	
			O5	4c	0.3016(238)	0.6920(62)	0.25	1	
			O6	8d	0.0370(132)	0.7872(43)	0.6162(70)	1	
			O7	8d	0.9263(115)	0.7360(71)	0.1045(53)	1	
33%	*R*3*c*	$a = 5.5354(1)$	Bi/Sm	6a	0	0	0	1.22(2)	$R_B = 1.953$
		$c = 13.6585(3)$	Fe	6a	0	0	0.2219(7)	0.49(7)	
			O	18b	0.4500(66)	0.0034(50)	0.9643(17)	1	

dx.doi.org/10.1021/ic402041p | *Inorg. Chem.* 2013, 52, 10698−10704

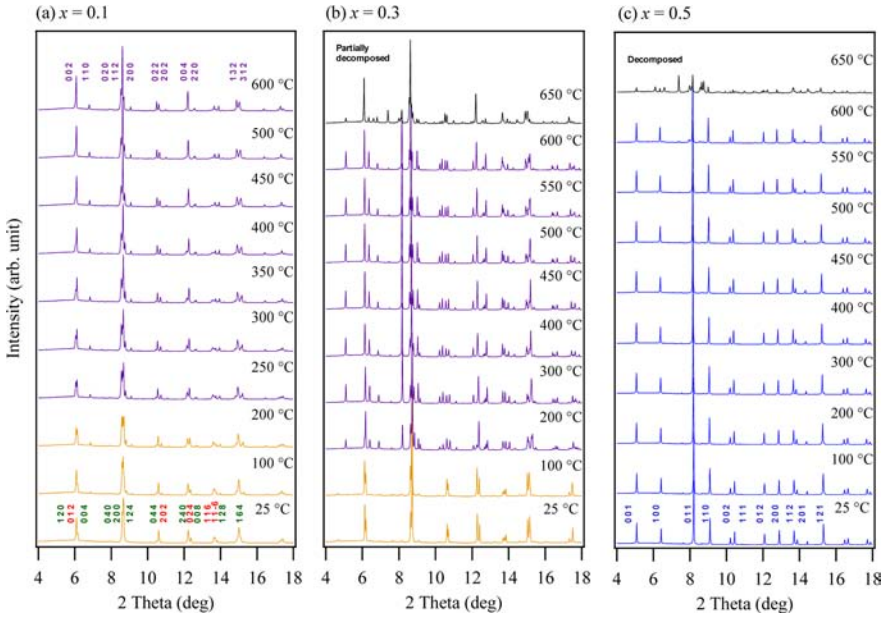

Figure 5. Temperature dependence of SXRD patterns of (a) $Bi_{0.9}Sm_{0.1}Fe_{0.9}Co_{0.1}O_3$, (b) $Bi_{0.9}Sm_{0.1}Fe_{0.7}Co_{0.3}O_3$, and (c) $Bi_{0.9}Sm_{0.1}Fe_{0.5}Co_{0.5}O_3$. The wavelength ($\lambda$) was 0.41918 Å. Green, red, purple, and blue notations represent Miller indices of $PbZrO_3$-type orthorhombic, $BiFeO_3$-type rhombohedral, $GdFeO_3$-type orthorhombic, and $BiCoO_3$-type tetragonal phases, respectively.

x increased, and the c/a ratio of the tetragonal cell increased as x increased. These tendencies are the same as those of the rhombohedral ($x \leq 0.2$) and tetragonal ($x \geq 0.4$) $BiFe_{1-x}Co_xO_3$.[7] Interestingly, the lattice parameters and the c/a ratio were less sensitive to the Sm substitution for Bi. This behavior is quite different from that of Sr-substituted $PbTiO_3$, where Sr substitution substantially decreased the c/a ratio.[42]

Figure 5 shows the SXRD patterns for the $Bi_{0.9}Sm_{0.1}Fe_{1-x}Co_xO_3$ (x = 0.10, 0.30, and 0.50) samples at elevated temperatures. The x = 0 sample had an antipolar $PbZrO_3$-type structure at room temperature. It changed to the ferroelectric $BiFeO_3$-type structure and finally to the paraelectric $GdFeO_3$-type structure upon heating, as previously reported.[28,29] In comparison, the $BiFeO_3$-type phase was not present as a single phase for the x = 0.10 sample at any temperature studied. Both $PbZrO_3$- and $BiFeO_3$-type phases coexisted at RT. A $GdFeO_3$-type structure appeared at around 200 °C and coexisted with the $PbZrO_3$-type phase below 300 °C. An orthorhombic $GdFeO_3$-type phase is commonly found as a paraelectric phase of $BiMO_3$ (M is a 3d transition metal) under a high-temperature or high-pressure condition.[43] For the x = 0.50 sample, only the tetragonal $BiCoO_3$-type phases were present below the decomposition temperature of 650 °C. At the intermediate composition (x = 0.30), a tetragonal $BiCoO_3$-type structure appeared at around 200 °C and coexisted with the $GdFeO_3$-type phase.

To investigate the effect of Sm substitution on the structure of $BiCoO_3$-type tetragonal phase, Rietveld analyses were performed on the SXRD patterns of $BiFe_{0.5}Co_{0.5}O_3$ and $Bi_{0.9}Sm_{0.1}Fe_{0.5}Co_{0.5}O_3$ at RT. As shown in Figure 6, both patterns were fit well for a polar *P4mm* model with large c/a ratios of 1.2614(1) and 1.2612(1) for $BiFe_{0.5}Co_{0.5}O_3$ and $Bi_{0.9}Sm_{0.1}Fe_{0.5}Co_{0.5}O_3$, respectively. Their spontaneous polarization calculated on the basis of structural parameters summarized in Table 2 by assuming a point-charge model were 128 and 122 μC/cm, respectively. Sm substitution on the

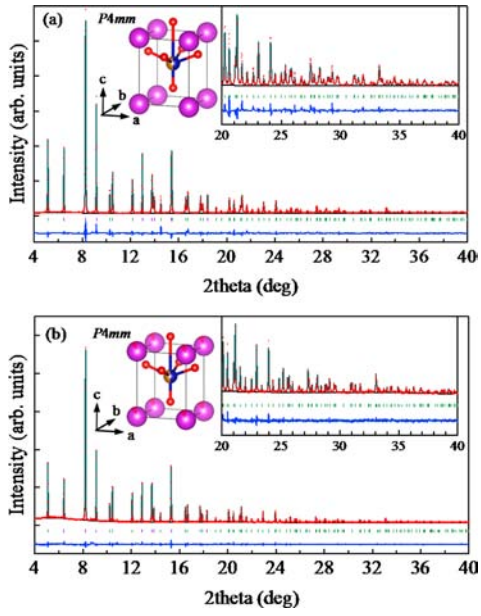

Figure 6. Observed, calculated, and difference synchrotron X-ray powder diffraction (SXRD) patterns and crystal structures of (a) $BiFe_{0.5}Co_{0.5}O_3$ and (b) $Bi_{0.9}Sm_{0.1}Fe_{0.5}Co_{0.5}O_3$ at room temperature. The wavelengths (λ) were (a) 0.42274 and (b) 0.42006 Å.

$BiCoO_3$-type structure showed little impact on the $BiCoO_3$-type tetragonal structure.

On the basis of the high-temperature XRD results, we constructed a tentative phase diagram, shown in Figure 7, with that for $BiFe_{1-x}Co_xO_3$ for comparison as an inset. The Sm substitution lowered the T_C of the $BiFeO_3$-type ferroelectric phase for x = 0. However, at the same time, the stable region of the $BiFeO_3$-type phase in the composition−temperature phase diagram drastically shrunk. The phases observed for the Co-substituted samples ($0.05 \leq x \leq 0.35$) at RT were the mixture of the $BiFeO_3$-type and antiferroelectric $PbZrO_3$-type phases.

dx.doi.org/10.1021/ic402041p | *Inorg. Chem.* 2013, 52, 10698−10704

Table 2. Structural Parameters for $BiFe_{0.5}Co_{0.5}O_3$ and $Bi_{0.9}Sm_{0.1}Fe_{0.5}Co_{0.5}O_3$ Refined by Rietveld Analysis of SXRD Patterns Collected at Room Temperature

Sm	cell (Å)	atom	Wyck	x	y	z	B	R factor (%)
0%	a = 3.7403(1)	Bi	1a	0	0	0	0.88(2)	R_{wp} = 6.158
	c = 4.7179(1)	Fe/Co	1b	0.5	0.5	0.5730(6)	0.73(6)	R_B = 1.333
		O1	1b	0.5	0.5	0.2018(26)	1.61(20)	
		O2	2c	0.5	0	0.7345(19)	1.61(20)	
10%	a = 3.7432(1)	Bi/Sm	1a	0	0	0	0.96(2)	R_{wp} = 4.620
	c = 4.7207(1)	Fe/Co	1b	0.5	0.5	0.5747(5)	0.45(5)	R_B = 2.553
		O1	1b	0.5	0.5	0.1858(23)	1.19(17)	
		O2	2c	0.5	0	0.7297(16)	1.19(17)	

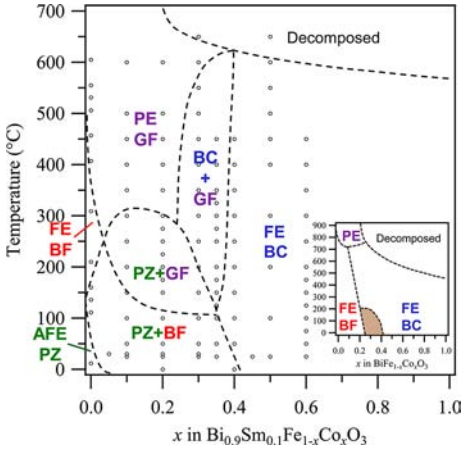

Figure 7. Composition−temperature phase diagram for the $Bi_{0.9}Sm_{0.1}Fe_{1-x}Co_xO_3$ system. Empty symbols represent measurement points. FE, AFE, and PE stand for ferroelectric, antiferroelectric, and paraelectric phases, respectively. BF, GF, PZ, and BC stand for the $BiFeO_3$-type rhombohedral, $GdFeO_3$-type orthorhombic, $PbZrO_3$-type orthorhombic, and $BiCoO_3$-type tetragonal phases, respectively. The diagram for the $BiFe_{1-x}Co_xO_3$ system[6] is shown as an inset for comparison. A monoclinic phase is stable in the shaded area.

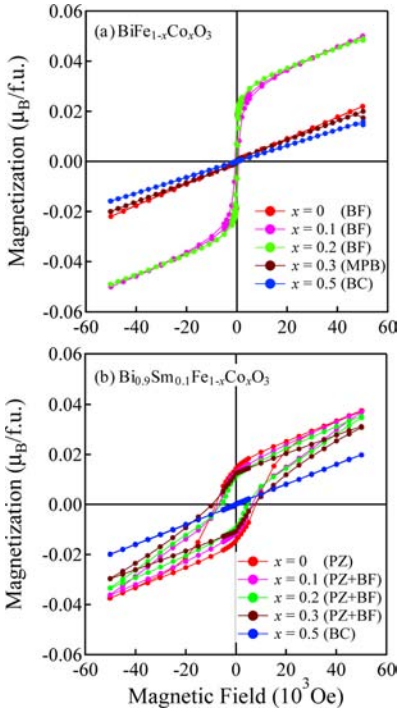

Figure 8. Field dependence of magnetization obtained for (a) $BiFe_{1-x}Co_xO_3$ (x = 0, 0.10, 0.20, 0.30, and 0.50) and (b) $Bi_{0.9}Sm_{0.1}Fe_{1-x}Co_xO_3$ (x = 0, 0.10, 0.20, 0.30, and 0.50) at room temperature. BF, BC, PZ, and MPB stand for $BiFeO_3$-type rhombohedral, $BiCoO_3$-type tetragonal, $PbZrO_3$-type orthorhombic, and monoclinic phases, respectively.

Contrary to our expectations, the tetragonal $BiCoO_3$-type phase was so stable that no reduction of T_C was observed. Furthermore, the monoclinic Cm phase disappeared. These results support our scenario in which the large tetragonal distortion of the $BiCoO_3$-containing phase was due to the Jahn−Teller distortion of a high-spin $t_{2g}^4e_g^2$ electronic configuration of Co^{3+}.[43] The tetragonal structure was stable because the Sm substitution for Bi did not affect the electronic state of the B-site cations. This is in contrast to the $BiFeO_3$-type structure destabilized by the substitution of Bi with Sm. However, it was insensitive to the B-site substitution, remaining unchanged by the replacement of Fe with Al.[44]

Let us move on to the magnetic property. Panels a and b of Figure 8 show the magnetization curves of $BiFe_{1-x}Co_xO_3$ (x = 0, 0.10, 0.20, 0.30, and 0.50) and $Bi_{0.9}Sm_{0.1}Fe_{1-x}Co_xO_3$ (x = 0, 0.10, 0.20, 0.30, and 0.50) at RT, respectively. Ferromagnetic behaviors were observed for the $R3c$ ferroelectric phase with substitution of Fe with Co ($BiFe_{1-x}Co_xO_3$ with x = 0.10 and 0.20). The spontaneous magnetization of 0.025 μ_B/f.u. was significantly large compared with that of Mn-substituted BFO.[36,38] Interestingly, the spontaneous moments were almost identical for the x = 0.10 and 0.20 samples. This suggests that the ferromagnetic moment was not coming from the ferrimagnetism or double-exchange mechanism but that the cycloidal spin structure of $BiFeO_3$ changed to another one that allows canted weak ferromagnetism. Indeed, a recent neutron powder diffraction study revealed that the magnetic structure of $BiFe_{0.8}Co_{0.2}O_3$ was collinear at room temperature.[45] On the other hand, no spontaneous magnetization was found for the samples with monoclinic (x = 0.30) and tetragonal (x = 0.50) structures. Assuming that their spin structures were C-type, the same as those of $BiCoO_3$, it is reasonable to assume that the magnetic moment pointing in the c-direction did not have a canting angle. The ferroelectricity and piezoelectricity of this composition were confirmed by our thin film studies.[14,46] The results described above indicate that Co-substituted rhombohedral $BiFeO_3$ is promising as a multiferroic material. In comparison, the $PbZrO_3$-type sample, $Bi_{0.9}Sm_{0.1}FeO_3$, showed a spontaneous moment without Co substitution, as previously reported.[47,48] It showed a relatively large coercive field, and the profile remained unaltered in the $PbZrO_3$-type and $BiFeO_3$-type mixed structure ($Bi_{0.9}Sm_{0.1}Fe_{1-x}Co_xO_3$ for which $0.10 \leq x \leq 0.30$). This is attributed to the $Pnam$ structure, quite different from the $R3c$ structure, rather than the magnetic property of

dx.doi.org/10.1021/ic402041p | Inorg. Chem. 2013, 52, 10698−10704

Sm atoms because Sm substitution had no impact on the paramagnetic behavior of the tetragonal structure.

CONCLUSION

The structure and magnetic properties of $BiFe_{1-x}Co_xO_3$ and $Bi_{0.9}Sm_{0.1}Fe_{1-x}Co_xO_3$ synthesized under high pressure were investigated. $BiFe_{1-x}Co_xO_3$ samples showed a compositional phase transition from a rhombohedral $BiFeO_3$-type structure ($0 \leq x \leq 0.20$) to a monoclinic structure ($x = 0.30$) and to a tetragonal $BiCoO_3$-type structure ($0.50 \leq x \leq 0.60$), while a mixture of a $PbZrO_3$-type structure with a $\sqrt{2}a \times 2\sqrt{2}a \times 4a$ and $BiFeO_3$-type structure of $Bi_{0.9}Sm_{0.1}Fe_{1-x}Co_xO_3$ ($0.05 \leq x \leq 0.35$) directly transformed to a $BiCoO_3$-type structure ($0.45 \leq x \leq 0.60$) via their mixed phase rather than a monoclinic phase. Ferroelectric $BiFe_{1-x}Co_xO_3$ ($x = 0.10$ and 0.20) and antiferroelectric $Bi_{0.9}Sm_{0.1}Fe_{1-x}Co_xO_3$ ($x = 0$, 0.10, 0.20, and 0.30) were found to possess spontaneous magnetic moments at room temperature. Co-substituted rhombohedral $BiFeO_3$, the ferroelectricity of which was confirmed for thin film samples, is promising as a multiferroic material.

ASSOCIATED CONTENT

Supporting Information

Composition dependence of the lattice parameters, c/a ratio, and unit cell volume of $Bi_{0.9}Sm_{0.1}Fe_{1-x}Co_xO_3$ at RT (Table S1) and temperature dependence of lattice parameters and c/a ratios of tetragonal $Bi_{0.9}Sm_{0.1}Fe_{0.5}Co_{0.5}O_3$ (Table S2 and Figure S1). This material is available free of charge via the Internet at http://pubs.acs.org.

AUTHOR INFORMATION

Corresponding Author

*E-mail: kubota.makoto@canon.co.jp.

Notes

The authors declare no competing financial interest.

ACKNOWLEDGMENTS

The authors express their thanks to Prof. Takao Sasagawa for his assistance in the magnetization measurements. This work was partially supported by the Elements Science and Technology Project of the Ministry of Education, Culture, Sports, Science and Technology, Japan, and by the Cabinet Office, Government of Japan, through its "Funding Program for Next Generation World-Leading Researchers" (GR032). The synchrotron radiation experiments were performed at SPring-8 with the approval of the Japan Synchrotron Radiation Research Institute (2012A1665 and 2012B1795).

REFERENCES

(1) Wang, J.; Neaton, J. B.; Zheng, H.; Nagarajan, V.; Ogale, S. B.; Liu, B.; Viehland, D.; Vaithyanathan, V.; Schlom, D. G.; Waghmare, U. V.; Spaldin, N. A.; Rabe, K. M.; Wuttig, M.; Ramesh, R. *Science* **2003**, *299*, 1719.
(2) Catalan, G.; Scott, J. F. *Adv. Mater.* **2009**, *21*, 2463.
(3) Kubel, F.; Schmid, H. *Acta Crystallogr.* **1990**, *B46*, 698.
(4) Lebeugle, D.; Colson, D.; Forget, A.; Viret, M. *Appl. Phys. Lett.* **2007**, *91*, 022907.
(5) Shvartsman, V. V.; Kleemann, W.; Haumont, R.; Kreisel, J. *Appl. Phys. Lett.* **2007**, *90*, 172115.
(6) Jaffe, B.; Cook, W. R.; Jaffe, H. *Piezoelectric Ceramics*; Academic Press: London, 1971.
(7) Azuma, M.; Niitaka, S.; Hayashi, N.; Oka, K.; Takano, M.; Funakubo, H.; Shimakawa, Y. *Jpn. J. Appl. Phys.* **2008**, *47*, 7579.
(8) Oka, K.; Koyama, T.; Ozaaki, T.; Mori, S.; Shimakawa, Y.; Azuma, M. *Angew. Chem., Int. Ed.* **2012**, *51*, 7977.
(9) Yasui, S.; Naganuma, H.; Okamura, S.; Nishida, K.; Yamamoto, T.; Iijima, T.; Azuma, M.; Morioka, H.; Saito, K.; Ishikawa, M.; Yamada, T.; Funakubo, H. *Jpn. J. Appl. Phys.* **2008**, *47*, 7582.
(10) Yasui, S.; Sakata, O.; Nakajima, M.; Utsugi, S.; Yazawa, K.; Yamada, T.; Funakubo, H. *Jpn. J. Appl. Phys.* **2009**, *48*, 09KD06.
(11) Yasui, S.; Yazawa, K.; Yamada, T.; Nishida, K.; Uchida, H.; Azuma, M.; Funakubo, H. *Jpn. J. Appl. Phys.* **2010**, *49*, 09MB04.
(12) Naganuma, H.; Miura, J.; Okamura, S. *Appl. Phys. Lett.* **2008**, *93*, 052901.
(13) Tho, N. T.; Kanashima, T.; Sohgawa, M.; Ricinschi, D.; Noda, M.; Okuyama, M. *Jpn. J. Appl. Phys.* **2010**, *49*, 09MB05.
(14) Nakamura, Y.; Kawai, M.; Azuma, M.; Kubota, M.; Shimada, M.; Aiba, T.; Shimakawa, Y. *Jpn. J. Appl. Phys.* **2011**, *50*, 031505.
(15) Miura, K.; Kubota, M.; Azuma, M.; Funakubo, H. *Jpn. J. Appl. Phys.* **2010**, *49*, 09ME07.
(16) Miura, K.; Kubota, M.; Azuma, M.; Funakubo, H. *Jpn. J. Appl. Phys.* **2009**, *48*, 09KF05.
(17) Yazawa, K.; Yasui, S.; Matsushima, M.; Uchida, H.; Funakubo, H. *Mater. Sci. Eng., B* **2010**, *173*, 14.
(18) Saito, Y.; Takao, H.; Tani, T.; Nonoyama, T.; Takatori, K.; Homma, T.; Nagaya, T.; Nakamura, M. *Nature* **2004**, *432*, 84.
(19) Shrout, T. R.; Zhang, S. J. *J. Electroceram.* **2007**, *19*, 111.
(20) Leontsev, S. O.; Eitel, R. E. *Sci. Technol. Adv. Mater.* **2010**, *11*, 044302.
(21) Leist, T.; Granzow, T.; Jo, W.; Rödel, J. *J. Appl. Phys.* **2010**, *108*, 014103.
(22) Fujino, S.; Murakami, M.; Anbusathaiah, V.; Lim, S. H.; Nagarajan, V.; Fennie, C. J.; Wuttig, M.; Salamanca-Riba, L.; Takeuchi, I. *Appl. Phys. Lett.* **2008**, *92*, 202904.
(23) Kan, D.; Palova, L.; Anbusathaiah, V.; Cheng, C. J.; Fujino, S.; Nagarajan, V.; Rabe, K. M.; Takeuchi, I. *Adv. Funct. Mater.* **2010**, *20*, 1108.
(24) Cheng, C. J.; Kan, D.; Lim, S. H.; McKenzie, W. R.; Munroe, P. R.; Salamanca-Riba, L. G.; Withers, R. L.; Takeuchi, I.; Nagarajan, V. *Phys. Rev. B* **2009**, *80*, 014109.
(25) Cheng, C. J.; Borisevich, A. Y.; Kan, D.; Takeuchi, I.; Nagarajan, V. *Chem. Mater.* **2010**, *22*, 2588.
(26) Emery, S. B.; Cheng, C. J.; Kan, D.; Rueckert, F. J.; Alpay, S. P.; Nagarajan, V.; Takeuchi, I.; Wells, B. O. *Appl. Phys. Lett.* **2010**, *97*, 152902.
(27) Borisevich, A. Y.; Eliseev, E. A.; Morozovska, A. N.; Cheng, C. J.; Lin, J. Y.; Chu, Y. H.; Kan, D.; Takeuchi, I.; Nagarajan, V.; Kalinin, S. V. *Nat. Commun.* **2012**, *3*, 775.
(28) Kubota, M.; Oka, K.; Nakamura, Y.; Yabuta, H.; Miura, K.; Shimakawa, Y.; Azuma, M. *Jpn. J. Appl. Phys.* **2011**, *50*, 09NE08.
(29) Kubota, M.; Oka, K.; Nakamura, Y.; Yabuta, H.; Miura, K.; Shimakawa, Y.; Azuma, M. *Funtai oyobi Funmatsu Yakin* **2012**, *59*, 239.
(30) Sosnowska, I.; Peterlin-Neumaier, T.; Steichele, E. *J. Phys. C: Solid State Phys.* **1982**, *15*, 4835.
(31) Kimura, T.; Goto, T.; Shintani, H.; Ishizaka, K.; Arima, T.; Tokura, Y. *Nature* **2003**, *426*, 55.
(32) Arima, T.; Goto, T.; Yamasaki, Y.; Miyasaka, S.; Ishii, K.; Tsubota, M.; Inami, T.; Murakami, Y.; Tokura, Y. *Phys. Rev. B* **2005**, *72*, 100102(R).
(33) Tokunaga, M.; Azuma, M.; Shimakawa, Y. *J. Phys. Soc. Jpn.* **2010**, *79*, 064713.
(34) Wardecki, D.; Przenioslo, R.; Sosnowska, I.; Skourski, Y.; Loewenhaupt, M. *J. Phys. Soc. Jpn.* **2008**, *77*, 103709.
(35) Ramazanoglu, M.; Laver, M.; Ratcliff, W.; Watson, S. M.; Chen, W. C.; Jackson, A.; Kothapalli, K.; Lee, S.; Cheong, S.-W.; Kiryukhin, V. *Phys. Rev. Lett.* **2011**, *107*, 207206.
(36) Azuma, M.; Kanda, H.; Belik, A. A.; Shimakawa, Y.; Takano, M. *J. Magn. Magn. Mater.* **2007**, *310*, 1177.
(37) Mandal, P.; Sundaresan, A.; Rao, C. N. R.; Iyo, A.; Shirage, P. M.; Tanaka, Y.; Simon, C.; Pralong, V.; Lebedev, O. I.; Caignaert, V.; Raveau, B. *Phys. Rev. B* **2010**, *82*, 100416.

(38) Belik, A. A.; Abakumov, A. M.; Tsirlin, A. A.; Hadermann, J.; Kim, J.; Van Tendeloo, G.; Takayama-Muromachi, E. *Chem. Mater.* **2011**, *23*, 4505.
(39) Puli, V. S.; Kumar, A.; Panwar, N.; Panwar, I. C.; Katiyar, R. S. *J. Alloys Compd.* **2011**, *509*, 8223.
(40) Izumi, F.; Momma, K. *Solid State Phenom.* **2007**, *130*, 15.
(41) Karimi, S.; Reaney, I. M.; Han, Y.; Pokorny, J.; Sterianou, I. *J. Mater. Sci.* **2009**, *44*, 5102.
(42) Kang, D. H.; Kim, J. H.; Park, J. H.; Yoon, K. H. *Mater. Res. Bull.* **2001**, *36*, 265.
(43) Oka, K.; Azuma, M.; Chen, W.; Yusa, H.; Belik, A.; Takayama-Muromachi, E.; Mizumaki, M.; Ishimatsu, N.; Hiraoka, N.; Tsujimoto, M.; Tucker, M. G.; Attfield, J. P.; Shimakawa, Y. *J. Am. Chem. Soc.* **2010**, *132*, 9438.
(44) Belik, A. A.; Wuernisha, T.; Kamiyama, T.; Mori, K.; Maie, M.; Nagai, T.; Matsui, Y.; Takayama-Muromachi, E. *Chem. Mater.* **2006**, *18*, 133.
(45) Sosnowska, I.; Azuma, M.; Przeniosło, R.; Wardecki, D.; Chen, W.; Oka, K.; Shimakawa, Y. *Inorg. Chem.* **2013**, submitted for publication.
(46) Nakamura, Y.; Kawai, M.; Azuma, M.; Shimakawa, Y. *Jpn. J. Appl. Phys.* **2010**, *49*, 051501.
(47) Khomchenko, V. A.; Paixao, J. A.; Shvartsman, V. V.; Borisov, P.; Kleemann, W.; Karpinsky, D. V.; Kholkin, A. L. *Scr. Mater.* **2010**, *62*, 238.
(48) Khomchenko, V. A.; Paixao, J. A.; Costa, B. F. O.; Karpinsky, D. V.; Kholkin, A. L.; Troyanchuk, I. O.; Shvartsman, V. V.; Borisov, P.; Kleemann, W. *Cryst. Res. Technol.* **2011**, *46*, 238.